

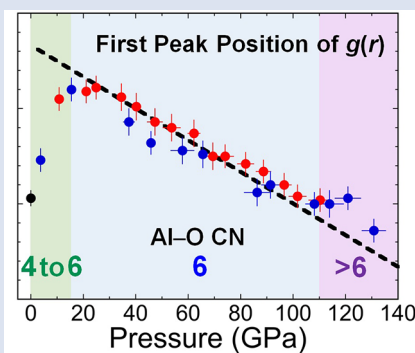
## ■ Ultrahigh pressure structural changes in a 60 mol. % $\text{Al}_2\text{O}_3$ –40 mol. % $\text{SiO}_2$ glass

I. Ohira<sup>1,2\*</sup>, Y. Kono<sup>1,3</sup>, Y. Shibazaki<sup>4,5</sup>, C. Kenney-Benson<sup>6</sup>, A. Masuno<sup>7</sup>, G. Shen<sup>6</sup>



doi: 10.7185/geochemlet.1913

### Abstract



Structure of an Al-containing silicate glass (60 mol. %  $\text{Al}_2\text{O}_3$ –40 mol. %  $\text{SiO}_2$ , A40S) is investigated up to 131 GPa, a pressure close to that of the Earth's core-mantle boundary, by using our recently developed double stage large volume cell. The first peak ( $r_1$ ) of the pair distribution function, which corresponds to T–O distance (T = Al, Si), rapidly increases below 16 GPa, indicating an increase of average coordination number (CN) of T–O from ~4 to 6. The  $r_1$  linearly decreases in the pressure range of 25–110 GPa, but it displays a slope change and becomes nearly constant above 110 GPa. The slope change may imply a structural change in the A40S glass around 110 GPa, and may be explained by the change in Al–O distance associated with the Al–O CN increase from 6 to >6 as predicted by molecular dynamics simulations (Ghosh and Karki, 2018). Our observations suggest an important role for aluminum in densification of aluminosilicate at the deep lower mantle, which might imply a dense aluminosilicate magma with negative buoyancy.

Received 11 September 2018 | Accepted 26 March 2019 | Published 3 May 2019

### Introduction

Pressure-induced structural change of silicate melts is one of the key factors in understanding the behaviour of silicate melts in the deep lower mantle to the core-mantle boundary (CMB), where the presence of silicate melt has been suggested by seismological studies as a cause of ultralow velocity zones (e.g., Garnero *et al.*, 1998). However, the structure of silicate melts at the ultrahigh pressure and high temperature conditions of the CMB is still poorly understood due to experimental challenges. Efforts have been made to understand pressure-induced structural changes in  $\text{SiO}_2$  glass, considered an analogue of silicate melts. Murakami and Bass (2010) found a kink in the pressure dependence of the shear wave velocity ( $dv_s/dP$ ) of a  $\text{SiO}_2$  glass at 140 GPa, and proposed a possible ultrahigh pressure structural change with an increase of the average Si–O coordination number (CN) to >6. Sato and Funamori (2010) investigated the structure of  $\text{SiO}_2$  glass and reported a constant Si–O CN of 6 from 35 GPa to 102 GPa. On the other hand, a recent structure measurement on  $\text{SiO}_2$  glass up to 172 GPa showed a gradual increase of the average Si–O CN from 6 to higher than 6 above 50 GPa (Prescher *et al.*, 2017), while

the trend of the gradual increase of Si–O CN is different from a sharp structural change as the kink observed in the  $dv_s/dP$  (Murakami and Bass, 2010).

Kinks in  $dv_s/dP$  have also been observed in  $\text{Al}_2\text{O}_3$ – $\text{SiO}_2$  glasses at 130 GPa (3.9 mol. %  $\text{Al}_2\text{O}_3$ –96.1 mol. %  $\text{SiO}_2$  glass) and at 116 GPa (20.5 mol. %  $\text{Al}_2\text{O}_3$ –79.5 mol. %  $\text{SiO}_2$  glass) (Ohira *et al.*, 2016). Ohira *et al.* (2016) suggested that incorporation of Al lowers the pressure condition of the ultrahigh pressure structural change, and indicated the role of aluminum in the structural change of aluminosilicate melts in the deep lower mantle. In fact, the composition of the melt generated by partial melting of a mid-ocean ridge basalt (MORB) at around 100 GPa contains a significant amount of  $\text{Al}_2\text{O}_3$  (~20 wt. % or ~13 mol. %) (Pradhan *et al.*, 2015). Therefore, an understanding of the pressure-induced structural changes in aluminosilicate systems is important in determining the nature of such melts in the CMB region. However, direct structure measurements on aluminosilicate glasses have been limited to <30 GPa (e.g., Drewitt *et al.*, 2015), and pressure-induced structural changes of Al–O at the pressure condition in the deep lower mantle have not been experimentally studied. In this study, we experimentally determined the pair distribution functions of a 60

1. Geophysical Laboratory, Carnegie Institution of Washington, Argonne, IL 60439, USA
  2. Department of Earth and Planetary Materials Science, Graduate School of Science, Tohoku University, Sendai 980-8578, Japan
  3. Geodynamics Research Center, Ehime University, Ehime 790-8577, Japan
  4. Frontier Research Institute for Interdisciplinary Sciences, Tohoku University, Aoba-ku, Sendai 980-8578, Japan
  5. International Center for Young Scientists, National Institute for Materials Science, Tsukuba 305-0047, Japan
  6. High Pressure Collaborative Access Team, X-ray Science Division, Argonne National Laboratory, Argonne, IL 60439, USA
  7. Graduate School of Science and Technology, Hirosaki University, Hirosaki 036-8561, Japan
- \* Corresponding author (email: itaru.ohira@gmail.com)



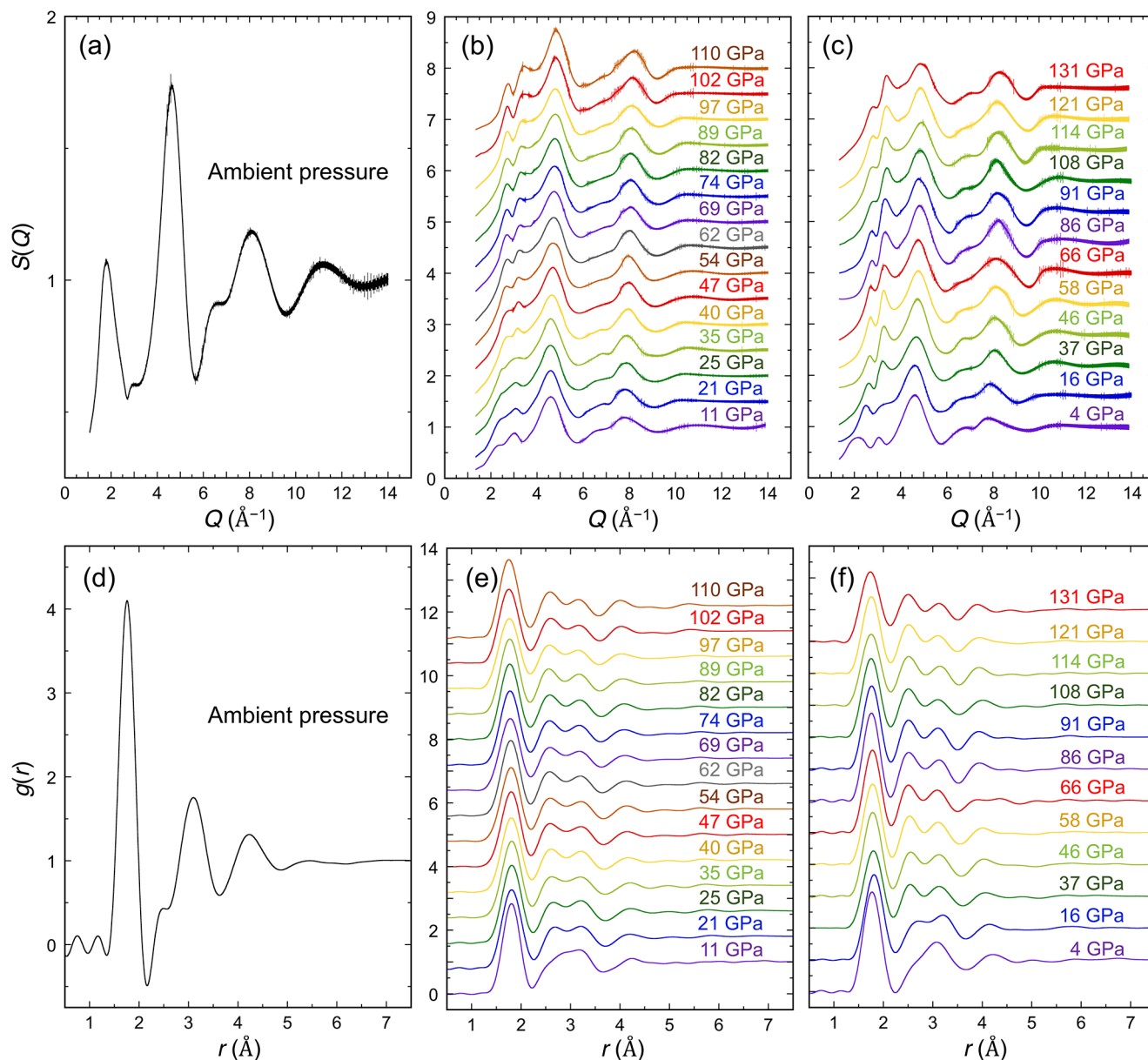


**Figure 1** Structure factors,  $S(Q)$ , determined at the  $Q$  range up to  $14 \text{ \AA}^{-1}$  and pair distribution functions,  $g(r)$ , of the A40S glass up to 131 GPa. (a)  $S(Q)$  at ambient condition. (b–c)  $S(Q)$  at high pressures displayed by a vertical offset of 0.5 and 0.6 in (b) for experiment 1 and (c) for experiment 2, respectively. (d)  $g(r)$  at ambient condition. (e–f)  $g(r)$  at high pressures displayed by a vertical offset of 0.8 and 1.0 in (e) for experiment 1 and (f) for experiment 2, respectively.

mol. %  $\text{Al}_2\text{O}_3$ –40 mol. %  $\text{SiO}_2$  glass (hereafter A40S glass) up to 131 GPa, and found an ultrahigh pressure structural change in this glass at pressures above 110 GPa.

## Structure Measurement up to 131 GPa

Figure 1 shows structure factors,  $S(Q)$ , of the A40S glass up to 131 GPa (Fig. 1a–c), and the reduced pair distribution functions,  $g(r)$  (Fig. 1d–f). The first peak ( $r_1$ ) of  $g(r)$  is considered to represent the T–O (T = Al and Si) distance. Since Si–O and Al–O bond distances are very close (for example, 1.64  $\text{\AA}$  and 1.81  $\text{\AA}$ , respectively, in  $\text{CaAl}_2\text{Si}_2\text{O}_8$  glass calculated by Ghosh and Karki, 2018), these bond distances are not resolvable even in the measurements at ambient pressure (e.g., Okuno *et al.*, 2005; Ohira *et al.*, 2016). Our observed  $r_1$  at ambient pressure ( $1.753 \pm 0.004 \text{ \AA}$ ) is consistent with that reported in a previous ambient pressure study ( $1.76 \pm 0.01 \text{ \AA}$  with T–O CN of  $4.3 \pm 0.1$ ; Okuno *et al.*, 2005). At ambient pressure, we observed that

there is a single second peak at  $\sim 3.1 \text{ \AA}$  with a shoulder peak at  $\sim 2.5 \text{ \AA}$ , while it changes to two distinct peaks above 16 GPa ( $r_2$  at  $\sim 2.5$ – $2.6 \text{ \AA}$  and  $r_3$  at  $\sim 3.1$ – $3.2 \text{ \AA}$ ). The basic feature of  $g(r)$  in the A40S glass above 16 GPa is similar to that of  $\text{SiO}_2$  glass with 6-fold coordinated structure at high pressures (Sato and Funamori, 2010; Prescher *et al.*, 2017), while the peak positions are different due to the difference between the Al–O and Si–O distances.

Figure 2 shows pressure dependences of  $r_1$ ,  $r_2$ , and  $r_3$  of the A40S glass, with the numerical data summarised in Table 1.  $r_1$  rapidly increases with increasing pressure at pressures below 16 GPa, and then almost linearly decreases with increasing pressure in the pressure range between 25 and 102 GPa (Fig. 2a). The slope of  $r_1$  changes with pressure at 25–102 GPa is similar to those of the Si–O bond distance in  $\text{SiO}_2$  glass with Si–O CN of  $\sim 6$  at 35–102 GPa (Sato and Funamori, 2010) and Al–O bond distance in  $\text{CaAl}_2\text{Si}_2\text{O}_8$  glass with Al–O CN of  $\sim 6$  at 41–105 GPa (Ghosh and Karki, 2018) (Fig. 2a). We find that  $r_1$  starts to deviate from the linear compression

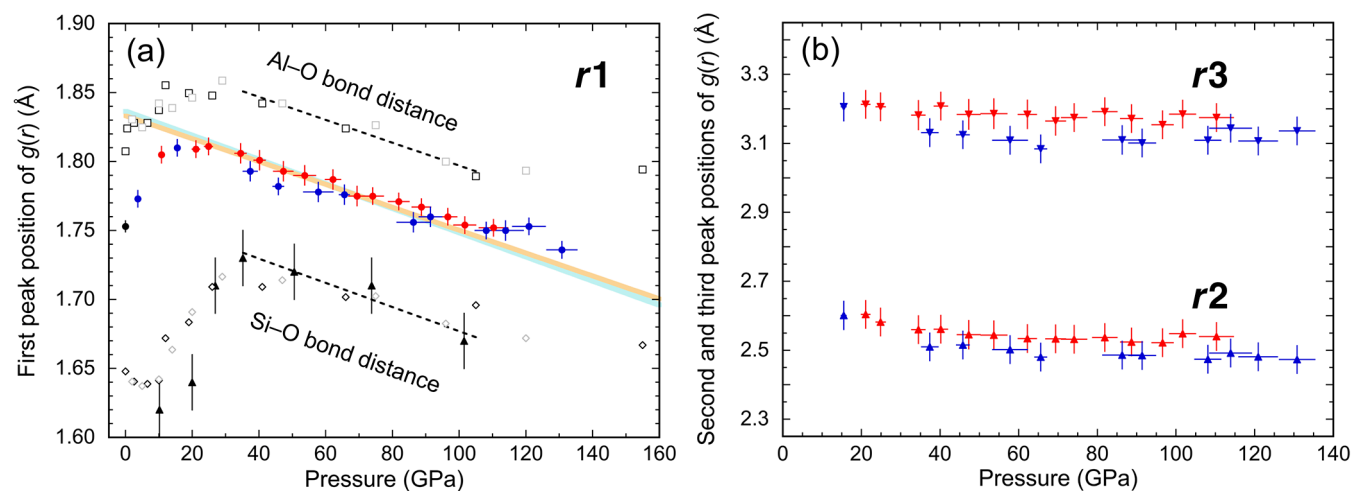


**Figure 2** The first ( $r_1$ ), second ( $r_2$ ), and third ( $r_3$ ) peak positions of  $g(r)$  of the A40S glass. (a) Red, blue, and black circles indicate the  $r_1$  determined in the high pressure experiments 1 and 2, and at ambient pressure, respectively. Triangles indicate the Si–O bond distance in  $\text{SiO}_2$  glass (Sato and Funamori, 2010). Open diamonds and squares indicate the Si–O and Al–O bond distance in  $\text{CaAl}_2\text{Si}_2\text{O}_8$  glass, respectively, simulated with 416 (black) and 208 (gray) atom simulation cells (Ghosh and Karki, 2018). The black dash lines are obtained from fitting for the Si–O and Al–O bond distances with CN =  $\sim 6$ . The light blue and orange lines are obtained from fitting the  $r_1$  of A40S glass at 35–102 GPa using the  $dr_{\text{Si-O}(6\text{CN})}/dP$  and the  $dr_{\text{Al-O}(6\text{CN})}/dP$ , respectively. The widths of lines indicate the fitting errors. (b) The  $r_2$  and  $r_3$  of the A40S glass determined in the experiments 1 (red) and 2 (blue), respectively.

trend above  $\sim 110$  GPa and becomes constant at 110–121 GPa (Fig. 2a). The determined  $r_2$  and  $r_3$  values show some differences between the two experiments (up to 0.1 Å), while these are almost within the experimental errors. It is noted, however, that the experimental results from both runs show monotonous changes in  $r_2$  and  $r_3$  between 16 and 131 GPa (Fig. 2b).

**Table 1** Experimental pressure conditions and the first ( $r_1$ ), second ( $r_2$ ), and third ( $r_3$ ) peak positions of  $g(r)$ .

Pressure (GPa)	$r_1$ (Å)	$r_2$ (Å)	$r_3$ (Å)
Ambient 0.0001	$1.753 \pm 0.004$		
Experiment 1			
10.8 $\pm$ 0.7	$1.805 \pm 0.006$		
21.1 $\pm$ 1.1	$1.809 \pm 0.006$	$2.604 \pm 0.040$	$3.213 \pm 0.040$
24.9 $\pm$ 1.2	$1.811 \pm 0.006$	$2.582 \pm 0.040$	$3.206 \pm 0.040$
34.5 $\pm$ 1.7	$1.806 \pm 0.007$	$2.560 \pm 0.040$	$3.182 \pm 0.042$
40.2 $\pm$ 1.7	$1.801 \pm 0.007$	$2.561 \pm 0.040$	$3.208 \pm 0.040$
47.3 $\pm$ 2.9	$1.793 \pm 0.007$	$2.545 \pm 0.041$	$3.184 \pm 0.043$
53.7 $\pm$ 3.3	$1.790 \pm 0.007$	$2.544 \pm 0.041$	$3.186 \pm 0.043$
62.2 $\pm$ 2.3	$1.787 \pm 0.007$	$2.534 \pm 0.040$	$3.184 \pm 0.041$
69.4 $\pm$ 2.5	$1.775 \pm 0.007$	$2.533 \pm 0.040$	$3.165 \pm 0.041$
74.1 $\pm$ 3.2	$1.775 \pm 0.006$	$2.532 \pm 0.040$	$3.175 \pm 0.040$
81.9 $\pm$ 3.1	$1.771 \pm 0.006$	$2.537 \pm 0.040$	$3.192 \pm 0.040$
88.7 $\pm$ 2.8	$1.767 \pm 0.006$	$2.524 \pm 0.040$	$3.172 \pm 0.040$
96.6 $\pm$ 2.7	$1.760 \pm 0.006$	$2.522 \pm 0.040$	$3.154 \pm 0.040$
101.7 $\pm$ 3.3	$1.754 \pm 0.006$	$2.548 \pm 0.040$	$3.185 \pm 0.040$
110.3 $\pm$ 4.3	$1.752 \pm 0.006$	$2.540 \pm 0.040$	$3.175 \pm 0.040$
Experiment 2			
3.7 $\pm$ 0.3	$1.773 \pm 0.006$		
15.5 $\pm$ 0.6	$1.810 \pm 0.006$	$2.601 \pm 0.041$	$3.206 \pm 0.041$
37.4 $\pm$ 2.1	$1.793 \pm 0.007$	$2.510 \pm 0.040$	$3.131 \pm 0.040$
45.8 $\pm$ 1.6	$1.782 \pm 0.006$	$2.515 \pm 0.040$	$3.125 \pm 0.040$
57.8 $\pm$ 4.4	$1.778 \pm 0.007$	$2.502 \pm 0.040$	$3.109 \pm 0.040$
65.6 $\pm$ 1.5	$1.776 \pm 0.007$	$2.480 \pm 0.040$	$3.084 \pm 0.040$
86.3 $\pm$ 4.9	$1.756 \pm 0.007$	$2.486 \pm 0.040$	$3.110 \pm 0.041$
91.4 $\pm$ 3.4	$1.760 \pm 0.007$	$2.485 \pm 0.040$	$3.101 \pm 0.040$
108.1 $\pm$ 3.3	$1.750 \pm 0.006$	$2.474 \pm 0.040$	$3.109 \pm 0.040$
113.9 $\pm$ 5.3	$1.750 \pm 0.007$	$2.492 \pm 0.040$	$3.144 \pm 0.040$
120.9 $\pm$ 4.3	$1.753 \pm 0.006$	$2.481 \pm 0.040$	$3.107 \pm 0.040$
130.8 $\pm$ 4.5	$1.736 \pm 0.006$	$2.473 \pm 0.040$	$3.136 \pm 0.040$

## Discussion

The A40S glass has a significantly higher content of Al than Si (Al/Si = 3), and therefore the behaviour of  $r_1$  is considered to mainly represent the Al–O distance. In fact, our observed behaviour of  $r_1$  at low pressure ( $< 25$  GPa) is consistent with the behaviour of Al–O distance reported in previous studies. Drewitt *et al.* (2015) showed an increase in Al–O distance in  $\text{CaAl}_2\text{O}_4$  glass with increasing pressure below 15 GPa, and then it displayed a slight decrease above 15 GPa. Along with the increase in Al–O distance, the average Al–O CN of  $\text{CaAl}_2\text{O}_4$  glass increases from 4 at ambient pressure to 6 at  $\sim 23.5$  GPa (Drewitt *et al.*, 2015). In addition, a recent simulation study for  $\text{CaAl}_2\text{Si}_2\text{O}_8$  glass found that the Al–O distance increases with increasing pressure below  $\sim 20$  GPa together with an increase of average Al–O CN (Ghosh and Karki, 2018) (Fig. 2a). The behaviour of the Al–O distance experimentally determined by Drewitt *et al.* (2015) and calculated by Ghosh and Karki (2018) is consistent with the change in  $r_1$  of the A40S glass obtained in this study (Fig. 2a). The increase of  $r_1$  below 16 GPa here is considered to represent an increase of Al–O CN from  $\sim 4$  to 6. The pressure condition where the Al–O CN reaches 6 is markedly lower than the pressure where the Si–O CN in  $\text{SiO}_2$  glass reaches 6 (at  $\sim 35$ – $50$  GPa: Sato and Funamori, 2010; Prescher *et al.*, 2017). Contrary to the behaviour of Al–O distance, Si–O distance decreases with increasing pressure up to  $\sim 10$ – $20$  GPa and then increases at  $\sim 20$ – $35$  GPa (Sato and Funamori, 2010; Ghosh and Karki, 2018) (Fig. 2a), which is markedly different from our observed  $r_1$ .

Above 25 GPa,  $r_1$  linearly decreases with increasing pressure, while it starts to deviate from a linear trend above around 110 GPa (Fig. 2a), which implies an existence of another structural change under ultrahigh pressure conditions. We find that the slope of the  $r_1$  changes in the A40S glass at 25–102 GPa shows a trend similar to the behaviour of Si–O and Al–O bond distances in  $\text{SiO}_2$  glass (Sato and Funamori, 2010) and  $\text{CaAl}_2\text{Si}_2\text{O}_8$  glass (Ghosh and Karki, 2018) with 6-fold coordinated structure, respectively. The Si–O bond distance shows a linear compression slope of  $dr_{\text{Si-O}(6\text{CN})}/dP = -8.77 \times 10^{-4}$  Å/GPa at 35–102 GPa (Fig. 2a). Similarly, the Al–O bond distance shows a slope of  $dr_{\text{Al-O}(6\text{CN})}/dP$  of  $-8.30 \times 10^{-4}$  Å/GPa (Fig. 2a), which is almost identical to the slope of Si–O. We therefore consider that the slope of the T–O bond distance (T = Si, Al)



with T–O CN of 6 in the A40S glass can be expressed by the same  $dr_1/dP$  as those of Si–O and Al–O bond distances. Indeed, when the  $r_1$  values are plotted with slopes of  $dr_1/dP$  being  $-8.77 \times 10^{-4} \text{ \AA/GPa}$  and  $-8.30 \times 10^{-4} \text{ \AA/GPa}$  at 34.5–101.7 GPa for SiO<sub>2</sub> and CaAl<sub>2</sub>Si<sub>2</sub>O<sub>8</sub> glasses, respectively, it appears that the behaviour of  $r_1$  in the A40S glass below 110 GPa can be well explained by the  $dr_1/dP$  slopes of the 6-fold coordinated structure. Above 110 GPa, however,  $r_1$  values deviate from the linear trends (Fig. 2a). Even if the linear range is selected at different pressure ranges (for example, at 35–131 GPa) or used for individual runs in experiment 1 and 2, the deviation of  $r_1$  from linear trends above 110 GPa can still be clearly identified (Fig. S-1). These results suggest a structural change at short range scale at ultrahigh pressures above ~110 GPa.

The kink in  $r_1$  of the A40S glass at 110 GPa in this study is consistent with the behaviour of Al–O distance in CaAl<sub>2</sub>Si<sub>2</sub>O<sub>8</sub> glass reported by Ghosh and Karki (2018). Ghosh and Karki (2018) showed a decrease of Al–O distance between ~10 and ~110 GPa, while it becomes constant or slightly increases above ~110 GPa in CaAl<sub>2</sub>Si<sub>2</sub>O<sub>8</sub> glass. The average Al–O CN of CaAl<sub>2</sub>Si<sub>2</sub>O<sub>8</sub> glass is constant at around 6 in a pressure range between 41 and 105 GPa, while it starts to increase to >6 above ~110 GPa (Ghosh and Karki, 2018). Thus, the kink in the pressure dependence of Al–O distance in CaAl<sub>2</sub>Si<sub>2</sub>O<sub>8</sub> glass at ~110 GPa is considered to represent the average Al–O CN increase from 6 to >6 (Ghosh and Karki, 2018). Although it is difficult for us to determine the average T–O CN in our A40S glass because of the lack of available density data for the A40S glass, the similarity between the Al–O distance change in Ghosh and Karki (2018) and the change in  $r_1$  in this study suggests an ultrahigh pressure structural change in the A40S glass to a more than 6-fold coordinated Al–O structure above 110 GPa. While  $r_1$  is nearly constant at 110–121 GPa, there is a decrease in  $r_1$  at 121–131 GPa. This decrease of  $r_1$  may imply that the change of Al–O CN may be completed at 131 GPa, in contrast to the theoretical prediction of a continuous Al–O CN increase to at least 155 GPa (Ghosh and Karki, 2018). However, data points are still limited, and further structural measurements at higher pressures are required to understand this question better. In addition, our observed decrease in  $r_1$  may be influenced by Si–O bond of the A40S glass, since the evolution of Si–O CN is still controversial in literature (for example, a gradual increase of Si–O CN to more than 6 above 50 GPa in Prescher *et al.*, 2017, while Si–O CN of less than 6 up to 155 GPa in Ghosh and Karki, 2018).

The pressure condition of the ultrahigh pressure structural change in the A40S glass observed in this study (110 GPa) is similar to the pressure condition where a kink in  $dv_S/dP$  is observed for Al<sub>2</sub>O<sub>3</sub>–SiO<sub>2</sub> glasses (116 GPa for 20.5 mol. % Al<sub>2</sub>O<sub>3</sub>–79.5 mol. % SiO<sub>2</sub> glass, Ohira *et al.*, 2016). The data suggest that the kink in the  $dv_S/dP$  is attributable to the increase of average Al–O CN to >6. Ohira *et al.* (2016) argued that incorporation of Al decreases the pressure of the sound velocity change of Al<sub>2</sub>O<sub>3</sub>–SiO<sub>2</sub> glasses. Therefore, the ultrahigh pressure structural change to more than 6-fold coordinated structure in Al<sub>2</sub>O<sub>3</sub>–SiO<sub>2</sub> system may also depend on the ratio of Si and Al.

The pressure condition of the Al–O CN change at 110 GPa is shallower than that of the CMB. Considering the similarity in the pressure-induced structural changes between aluminosilicate glass and melt at very high pressure conditions of the Earth's lower mantle (Sanloup, 2016), the Al–O CN change may occur in aluminosilicate melt in the CMB region and may have a significant influence on the behaviour of Al-rich aluminosilicate magmas generated by partial melting of MORB (Pradhan *et al.*, 2015). It is interesting to note that Al-rich glasses show different behaviour in density from those of Al-free silicate glasses. Petitgirard *et al.* (2015, 2017)

showed a similarity in density of SiO<sub>2</sub> and MgSiO<sub>3</sub> glasses at the pressure conditions of the Earth's lowermost mantle, which indicates a minor effect of SiO<sub>2</sub> content on the density of silicate glasses (Fig. S-2). On the other hand, we note that the density of CaAl<sub>2</sub>Si<sub>2</sub>O<sub>8</sub> glass (Ghosh and Karki, 2018) becomes higher than those of SiO<sub>2</sub> and MgSiO<sub>3</sub> glasses above 82 and 64 GPa, respectively (Fig. S-2), likely due to an average Al–O CN change to >6 while the average Si–O CN remains at 6. It has been known that densities of SiO<sub>2</sub> and MgSiO<sub>3</sub> glasses are lower than that of the Preliminary reference Earth model (PREM) (Dziewonski and Anderson, 1981) at the pressures of the CMB (Petitgirard *et al.*, 2017). The important role of Fe in the formation of silicate magma with density higher than PREM has been discussed in previous studies (*e.g.*, Petitgirard *et al.*, 2015, 2017; Karki *et al.*, 2018). A recent study showed that only highly Fe-rich melts (*e.g.*, ~0.35 of Fe/(Mg+Fe)) could be denser than the surrounding mantle (Karki *et al.*, 2018). However, to generate such a Fe-rich melt, very low partition coefficients ( $D_{\text{Fe}}^{\text{mineral/melt}}$ ) and low degree of partial melting are required (*e.g.*, Andrault *et al.*, 2017), while these parameters at ultrahigh pressure and high temperature conditions of the deep lower mantle are still under debate (*e.g.*, Andrault *et al.*, 2017). On the other hand, Fe-free CaAl<sub>2</sub>Si<sub>2</sub>O<sub>8</sub> glass has markedly higher density than SiO<sub>2</sub> and MgSiO<sub>3</sub> glasses above 100 GPa (Fig. S-2), which suggests an important densification role of average Al–O CN to more than 6 in the formation of dense magma at pressures near the CMB.

## Acknowledgements

We are grateful to the three anonymous reviewers for their comments that helped to improve the manuscript. High pressure experiments were performed at HPCAT (Sector 16), Advanced Photon Source (APS), Argonne National Laboratory. HPCAT operation is supported by DOE–NNSA under Award No. DE-NA0001974. The Advanced Photon Source is a U.S. Department of Energy (DOE) Office of Science User Facility operated for the DOE Office of Science by Argonne National Laboratory under Contract No. DE-AC02-06CH11357. This research is supported by JSPS overseas fellowships to IO and the National Science Foundation under Award No. EAR-1722495 to YK. GS acknowledges the support of DOE-BES/DMSE under Award DE-FG02-99ER45775. YS acknowledges the support of JSPS KAKENHI Grant Number 15K17784.

Editor: Wendy Mao

## Additional Information

Supplementary Information accompanies this letter at <http://www.geochemicalperspectivesletters.org/article1913>.



This work is distributed under the Creative Commons Attribution Non-Commercial No-Derivatives 4.0 License, which permits unrestricted distribution provided the original author and source are credited. The material may not be adapted (remixed, transformed or built upon) or used for commercial purposes without written permission from the author. Additional information is available at <http://www.geochemicalperspectivesletters.org/copyright-and-permissions>.

**Cite this letter as:** Ohira, I., Kono, Y., Shibazaki, Y., Kenney-Benson, C., Masuno, A., Shen, G. (2019) Ultrahigh pressure structural changes in a 60 mol. % Al<sub>2</sub>O<sub>3</sub>–40 mol. % SiO<sub>2</sub> glass. *Geochem. Persp. Let.* 10, 41–45.



## References

- ANDRAULT, D., BOLEFAN-CASANOVA, N., BOUHIFD, M.A., BOUJIBAR, A., GARBARINO, G., MANTHILAKE, G., MEZOUAR, M., MONTEUX, J., PARISIADIS, P., PESCE, G. (2017) Toward a coherent model for the melting behavior of the deep Earth's mantle. *Physics of the Earth and Planetary Interiors* 265, 67–81.
- DREWITT, J.W.E., JAHN, S., SANLOUP, C., DE GROUCHY, C., GARBARINO, G., HENNET, L. (2015) Development of chemical and topological structure in aluminosilicate liquids and glasses at high pressure. *Journal of Physics: Condensed Matter* 27, 105103.
- DZIEWONSKI, A.M., ANDERSON, D.L. (1981) Preliminary reference Earth model. *Physics of the Earth and Planetary Interiors* 25, 297–356.
- GARNERO, E.J., REVENAUGH, J., WILLIAMS, Q., LAY, T., KELLOGG, L.H. (1998) Ultralow velocity zone at the core-mantle boundary. In: Gurnis, M., Wyssession, M.E., Knittle, E., Buffett, B.A. (Eds.) *The core-mantle boundary region*. The American Geophysical Union, Washington, D.C., 319–334.
- GHOSH, D.B., KARKI, B.B. (2018) First-principles molecular dynamics simulations of anorthite (CaAl<sub>2</sub>Si<sub>2</sub>O<sub>8</sub>) glass at high pressure. *Physics and Chemistry of Minerals* 45, 575–587.
- KARKI, B.B., GHOSH, D.B., MAHARJAN, C., KARATO, S.-I., PARK, J. (2018) Density-pressure profiles of Fe-bearing MgSiO<sub>3</sub> liquid: effects of valence and spin states, and implications for the chemical evolution of the lower mantle. *Geophysical Research Letters* 45, 3959–3966.
- MURAKAMI, M., BASS, J.D. (2010) Spectroscopic evidence for ultrahigh-pressure polymorphism in SiO<sub>2</sub> glass. *Physical Review Letters* 104, 025504.
- OHIRA, I., MURAKAMI, M., KOHARA, S., OHARA, K., OHTANI, E. (2016) Ultrahigh-pressure acoustic wave velocities of SiO<sub>2</sub>-Al<sub>2</sub>O<sub>3</sub> glasses up to 200 GPa. *Progress in Earth and Planetary Science* 3, 18.
- OKUNO, M., ZOTOV, N., SCHMÜCKER, M., SCHNEIDER, H. (2005) Structure of SiO<sub>2</sub>-Al<sub>2</sub>O<sub>3</sub> glasses: combined X-ray diffraction, IR and Raman studies. *Journal of Non-Crystalline Solids* 351, 1032–1038.
- PETITGIRARD, S., MALFAIT, W.J., SINMYO, R., KUPENKO, I., HENNET, L., HARRIES, D., DANE, T., BURGHAMMER, M., RUBIE, D.C. (2015) Fate of MgSiO<sub>3</sub> melts at core-mantle boundary conditions. *Proceedings of the National Academy of Sciences of the United States of America* 112, 14186–14190.
- PETITGIRARD, S., MALFAIT, W.J., JOURNAUX, B., COLLINGS, I.E., JENNINGS, E.S., BLANCHARD, I., KANTOR, I., KURNOSOV, A., COTTE, M., DANE, T., BURGHAMMER, M., RUBIE, D.C. (2017) SiO<sub>2</sub> glass density to lower-mantle pressures. *Physical Review Letters* 119, 215701.
- PRADHAN, G.K., FIQUET, G., SIEBERT, J., AUZENDE, A.-L., MORARD, G., ANTONANGELI, D., GARBARINO, G. (2015) Melting of MORB at core-mantle boundary. *Earth and Planetary Science Letters* 431, 247–255.
- PRESCHER, C., PRAKAPENKA, V.B., STEFANSKI, J., JAHN, S., SKINNER, L.B., WANG, Y. (2017) Beyond sixfold coordinated Si in SiO<sub>2</sub> glass at ultrahigh pressures. *Proceedings of the National Academy of Sciences of the United States of America* 114, 10041–10046.
- SANLOUP, C. (2016) Density of magmas at depth. *Chemical Geology* 429, 51–59.
- SATO, T., FUNAMORI, N. (2010) High-pressure structural transformation of SiO<sub>2</sub> glass up to 100 GPa. *Physical Review B* 82, 184102.

## ■ Ultrahigh-pressure structural changes in a 60 mol. % Al<sub>2</sub>O<sub>3</sub>–40 mol. % SiO<sub>2</sub> glass

I. Ohira, Y. Kono, Y. Shibazaki, C. Kenney-Benson, A. Masuno, G. Shen

### ■ Supplementary Information

The Supplementary Information includes:

- Material
- Method
- Figures S-1 to S-5
- Supplementary Information References

#### **Material**

The glass with composition of 60 mol. % Al<sub>2</sub>O<sub>3</sub>–40 mol. % SiO<sub>2</sub> was synthesised from a stoichiometric powder mixture by means of containerless levitation heating method at Hirosaki University, Japan. Blocks of silicate powders (1–2 mg) were levitated in oxygen using an aerodynamic levitator and heated by a 100 W-CO<sub>2</sub> laser. A small vitreous spheroid (~1–2 mm in diameter) was obtained by a cooling rate of a few hundreds of degrees per second. The synthesis of glasses using an aerodynamic levitation furnace is described elsewhere (Rosales-Sosa *et al.*, 2016). The synthesised spheroid was polished to ~150 µm thick of disk and divided into several pieces to put into the sample chamber.

#### **Method**

A double-stage large volume cell, developed in the 200-ton Paris–Edinburgh press at HPCAT of the Advanced Photon Source (Kono *et al.*, 2016, 2018), was used for the high-pressure experiments. The data at ambient pressure was measured without a high-pressure cell. We used a set of cup-shaped WC anvils as the first stage anvils and a set of (100)-oriented single crystal diamonds as the second stage anvils. We used diamond anvils with a 0.6 mm culet beveled to 0.8 mm diameter in experiment 1 and a 0.5 mm culet beveled to 0.7 mm diameter in experiment 2. An aluminum alloy (7075) or beryllium gasket with 150 µm thickness were used as outer gasket for the experiments 1 and 2, respectively. Cubic boron nitride + epoxy (10:1 in weight ratio) was used as the inner gasket inside the metal gasket. The initial sample diameter was 0.23 mm for experiment 1 and 0.20 mm for experiment 2. A piece of gold, used as a pressure marker, was placed at the edge of the glass sample to avoid contamination of the X-ray spectra of gold into that of glass sample. Pressures were determined by using the equation of state of gold (Tsuchiya, 2003). The 220, 311, 222, 400, 331, 420, and 422 reflections of gold were used for calculating the experimental pressures. The X-ray spectra of the gold were collected before and after each structure measurement of the glass sample, except for two pressure points at 4 and 16 GPa where pressure was determined only before or after the structure measurement, respectively. The pressure values are summarised in Table 1



together with the peak positions of  $g(r)$ . Pressure generation as a function of oil load of the Paris–Edinburgh press was shown in Figure S-3. The pressure errors are defined as two-sigma that is calculated from the pressure values determined from the seven reflections measured before and after sample measurements (Table 1). In addition, the pressure difference between the center and the edge of the sample was 8 GPa at the experimental pressure of 108 GPa.

Structure factor,  $S(Q)$ , of the 60 mol. %  $\text{Al}_2\text{O}_3$ –40 mol. %  $\text{SiO}_2$  glass was measured using the multi-angle energy dispersive X-ray diffraction technique (Kono *et al.*, 2014). The incident white X-rays were focused to 0.009 mm (full width at half maximum) in horizontal direction and 0.016 mm in vertical direction in the experiment 1, and to 0.005 mm in horizontal direction and 0.008 mm in vertical direction in the experiment 2 by using a 200-mm-long Pt-coated K-B mirror with an incident angle of 1.25 mrad, which produces an energy cutoff at  $\sim 65$  keV. We collected series of energy dispersive X-ray diffraction patterns using a Ge solid-state detector (Canberra) at two-theta angles of 4.6°, 6.6°, 8.1°, 10.6°, 13.6°, 17.1°, 21.1°, and 28.1° for the experiment 1, 3.6°, 4.6°, 6.1°, 8.2°, 10.7°, 13.7°, 17.2°, 21.2°, and 27.2° for the experiment 2, and 3.1°, 4.1°, 5.1°, 7.1°, 9.1°, 12.1°, 16.1°, 22.1°, 28.1°, and 35.1° for the ambient pressure measurement. The  $S(Q)$  was determined from the collected energy dispersive X-ray diffraction patterns using the aEDXD program developed by Changyong Park (Kono *et al.*, 2014). Since the minimum  $Q$  range ( $Q_{\min}$ ) is different between the experiments 1 and 2 due to the difference of the lowest two-theta angle in the measurement, we slightly extrapolated the  $S(Q)$  of the experiment 1 from 1.67  $\text{\AA}^{-1}$  to the  $Q_{\min}$  (1.35  $\text{\AA}^{-1}$ ) of the experiment 2 by using a liner extrapolation for consistent analysis of the pair distribution function. A similar extrapolation method has been used in a previous study (Prescher *et al.*, 2017).

The pair distribution function,  $g(r)$ , was calculated by Fourier Transform of  $S(Q)$ :

$$g(r) = 1 + \frac{1}{2\pi^2 n} \int_{Q_{\min}}^{Q_{\max}} Q[S(Q) - 1] \sin(Qr) dQ \quad (\text{Eq. S-1})$$

where  $n$  is the number density. To determine the  $g(r)$  of the A40S glass, we used the second-order polynomial curve of  $\text{SiO}_2$  glass for the data at less than 57.8 GPa ( $\rho = -0.000538 \times P^2 + 0.076284 \times P + 2.203$ ) and the fourth-order Birch–Murnaghan equation of state of the  $\text{SiO}_2$  glass for the data at more than 62.2 GPa ( $\rho_0 = 3.95 \text{ g/cm}^3$ ,  $K_0 = 183.3 \text{ GPa}$ ,  $K_0' = 5.0$ ) (Petitgirard *et al.*, 2017). The Kaplow-type correction using an optimisation procedure (Shen *et al.*, 2003) was applied in determining final structure factors and pair distribution functions. We repeated the optimisation iterations five times. The peak positions in  $g(r)$  were fitted with Gaussian function.

Results of  $g(r)$  and the resultant peak positions of  $g(r)$  ( $r_1$ ,  $r_2$ , and  $r_3$ ) may be influenced by the range of  $Q$  of  $S(Q)$ . In order to evaluate the influence of  $Q$  range on the results of  $g(r)$  and the peak positions, we conducted the analysis of  $g(r)$  at ambient conditions using various  $Q$  ranges (the maximum  $Q$  range,  $Q_{\max} = 10, 11, 12, 13, 14, 15, 16, 17 \text{ \AA}^{-1}$ ). The results are shown in Supplementary Figures (Figs. S-4 and S-5). The peak positions of  $g(r)$  are similar when  $Q_{\max}$  are higher than 12  $\text{\AA}^{-1}$ , while the  $r_1$ – $r_3$  become scattered when  $Q_{\max}$  are less than  $\sim 11 \text{ \AA}^{-1}$ . These data clearly show that our analysis with the  $Q_{\max} = 14 \text{ \AA}^{-1}$  is of high enough quality to determine the peak positions of the  $g(r)$ . We defined the errors of the  $r_1$ – $r_3$  at ambient conditions as a square-root of sum of squares of  $3\sigma$  of the peak positions of the analyses using the  $Q_{\max}$  of 12–17  $\text{\AA}^{-1}$  and  $3\sigma$  of peak-fitting errors (Table 1). The same procedure was applied to high pressure data with the  $Q_{\max}$  of 10, 11, 12, 13, 14  $\text{\AA}^{-1}$  (Fig. S-5). At high  $Q_{\max}$  between 11 and 14  $\text{\AA}^{-1}$ ,  $r_1$  and  $r_3$  values are within the error bar, although the  $r_2$  shows slightly higher value at  $Q_{\max} = 11$ . At  $Q_{\max} = 10 \text{ \AA}^{-1}$ , all the  $r_1$ – $r_3$  show deviation from those obtained at the  $Q_{\max}$  higher than 11. With consideration of these uncertainties, the fluctuation of the  $r_1$ – $r_3$  in the analysis of  $Q_{\max} = 11, 12, 13, 14 \text{ \AA}^{-1}$  are adopted as the errors of the  $r_1$ – $r_3$  due to  $Q_{\max}$ . The largest  $3\sigma$  of each peak position at the  $Q_{\max}$  of 11–14  $\text{\AA}^{-1}$  is 0.006  $\text{\AA}$  for  $r_1$ , 0.039  $\text{\AA}$  for  $r_2$ , and 0.040  $\text{\AA}$  for  $r_3$ , and we adopted it as the error due to  $Q_{\max}$  in all high pressure measurement. Then, we calculated square-root of sum of squares of the  $3\sigma$  due to  $Q_{\max}$  and the  $3\sigma$  of peak-fitting, as the errors of  $r_1$ – $r_3$  at high pressure conditions (Table 1).



Supplementary Figures

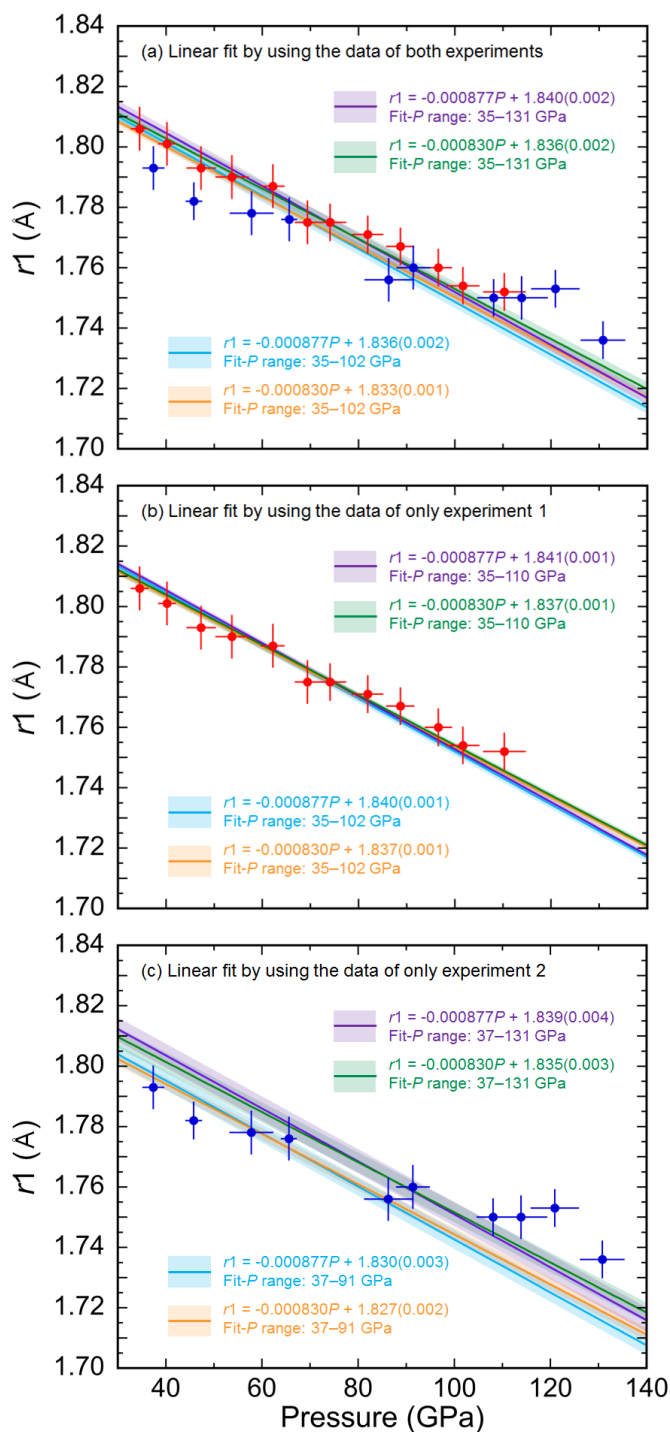


**Figure S-1** The first ( $r1$ ) peak position of  $g(r)$  of the A40S glass with the fitting lines. Red and blue circles indicate the  $r1$  determined in the high-pressure experiments 1 and 2, respectively. **(a)** Linear fit for  $r1$  obtained from both of the two experiments. The light blue and orange lines are obtained from fitting for the  $r1$  of A40S glass at 35–102 GPa, using the  $dr1/dP$  values of the Si–O and Al–O bond distances with CN of 6 ( $-8.77 \times 10^{-4}$  Å/GPa, Sato and Funamori, 2010;  $-8.30 \times 10^{-4}$  Å/GPa, Ghosh and Karki, 2018, respectively), as same as the Figure 2a. The purple and green lines are obtained from fitting at 35–131 GPa using the same  $dr1/dP$  values. **(b)** Linear fit for  $r1$  obtained from only the experiment 1. Two fitting ranges (35–102 GPa and 35–110 GPa) were applied using the  $dr1/dP$  values same as (a). **(c)** Linear fit for  $r1$  obtained from only the experiment 2. Two fitting ranges (37–91 GPa and 37–131 GPa) were applied using the  $dr1/dP$  values same as (a). The shaded bands surrounding the lines indicate the fitting errors. When the data up to 131 GPa are fit, the fitting lines show slightly higher values than those determined by using the data up to 102 GPa. Nevertheless, the  $r1$  above 110 GPa shows deviation from the fitting lines. In addition, since there is somewhat difference in the  $r1$  of up to 0.013 Å between the two experiments, we evaluated the linear fit in each experiment. Even if the plot for the  $r1$  is fit in the experiment 1 and 2, individually (b, c), the deviation of the  $r1$  above 110 GPa can also be clearly identified.



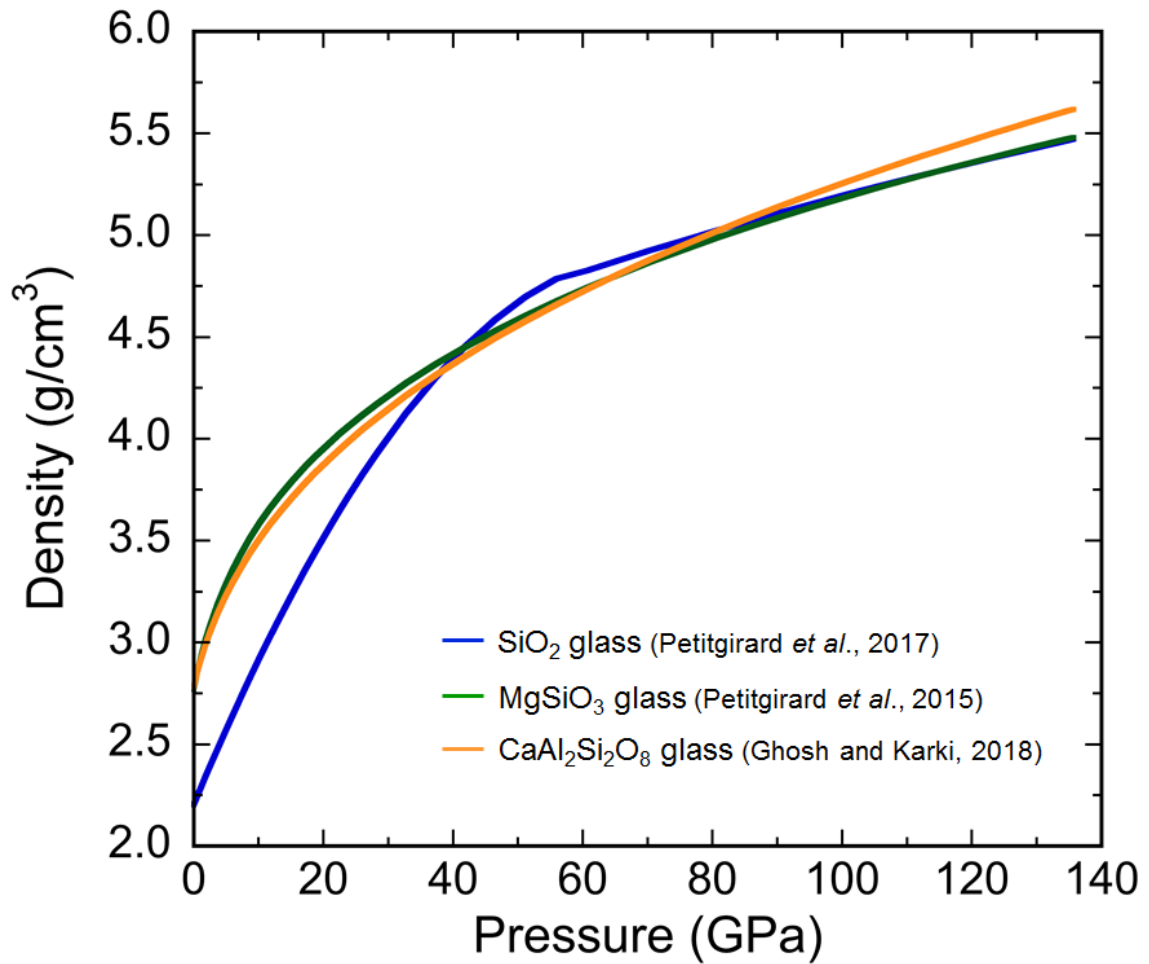


**Figure S-2** Density of SiO<sub>2</sub> (blue: Petitgirard *et al.*, 2017), MgSiO<sub>3</sub> (green: Petitgirard *et al.*, 2015), and CaAl<sub>2</sub>Si<sub>2</sub>O<sub>8</sub> (orange: Ghosh and Karki, 2018) glasses reported in the previous studies.

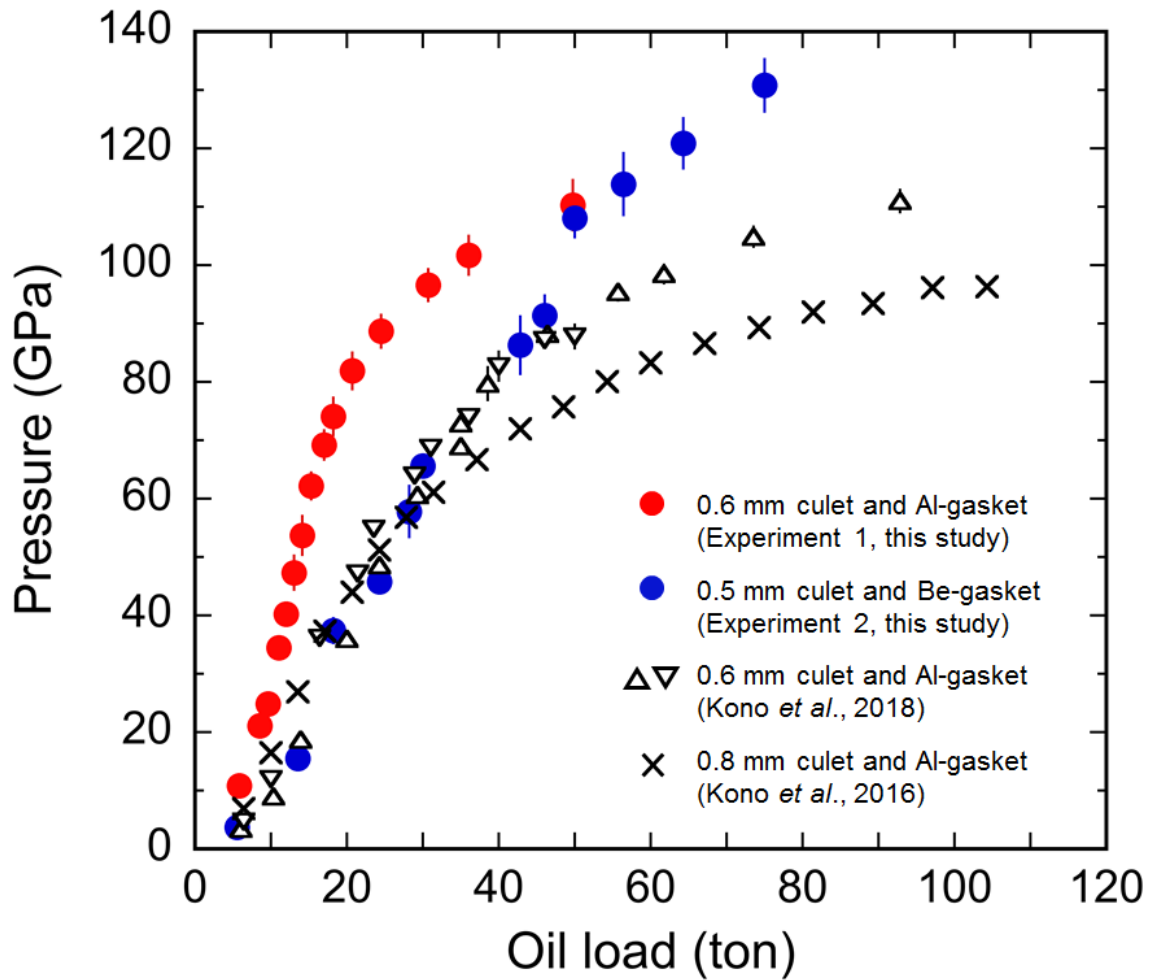


**Figure S-3** Pressure generation as a function of oil load of the large volume press. Red (experiment 1) and blue (experiment 2) solid circles represent pressure conditions of the structure measurements in this study. Black symbols represent pressure generation of the previous studies (Kono *et al.*, 2016, 2018).



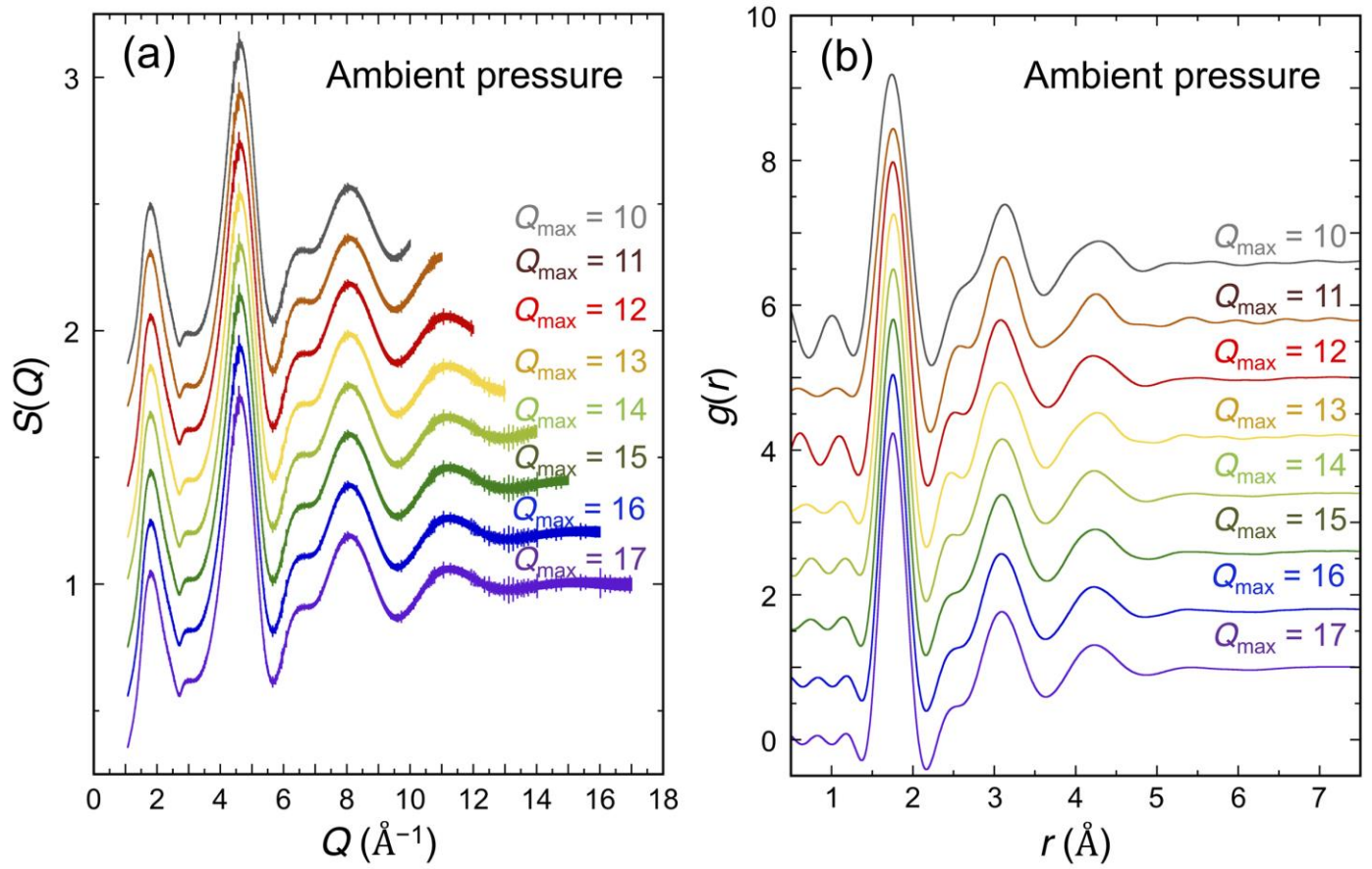


**Figure S-4** Results of (a)  $S(Q)$  and (b)  $g(r)$  of A40S glass analysed by using different  $Q_{\text{max}}$  at ambient condition. (a)  $S(Q)$  are displayed by a vertical offset of 0.2. (b)  $g(r)$  are displayed by vertical offset of 0.8.

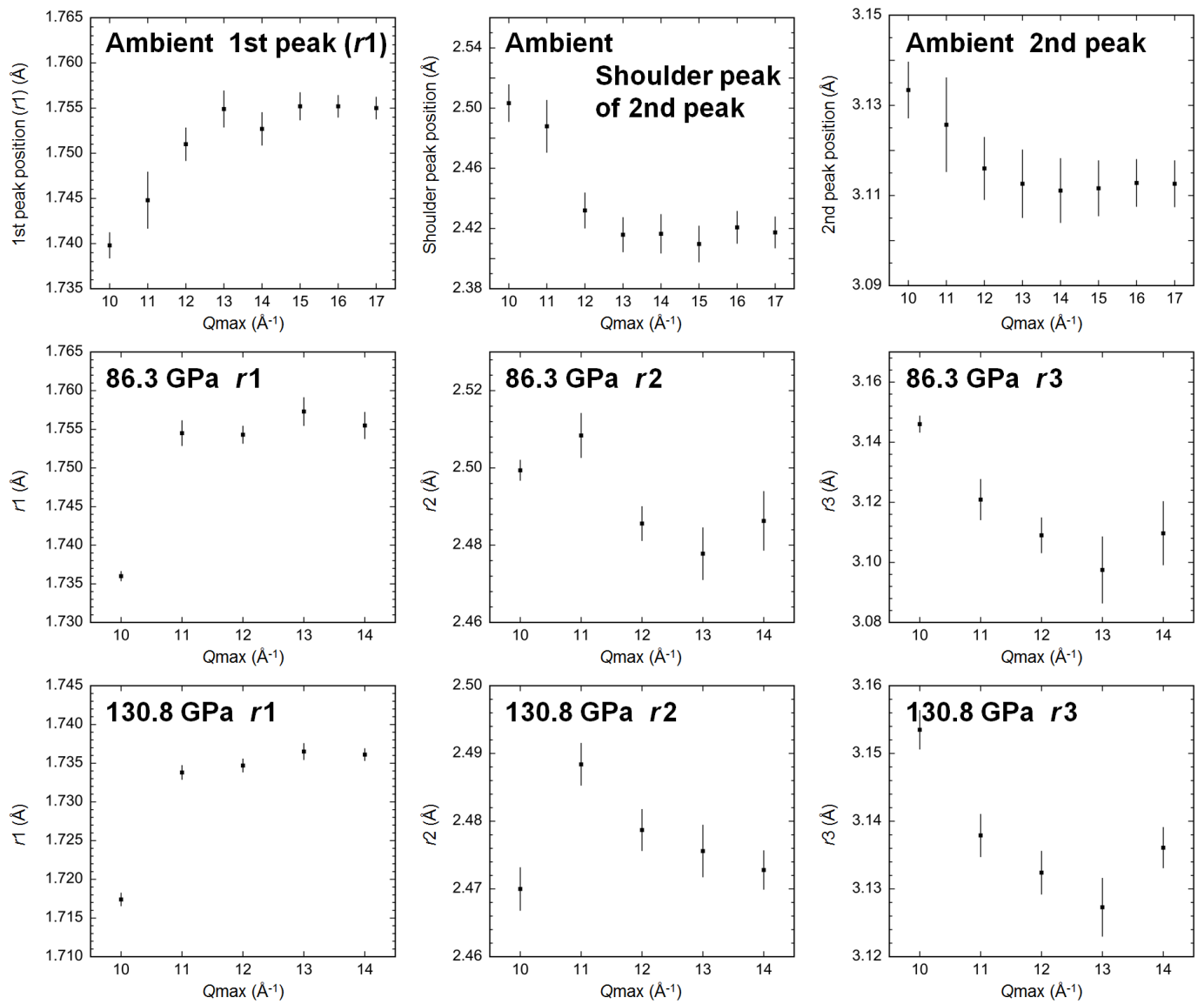


**Figure S-5** Variation of the peak positions as a function of  $Q_{max}$  evaluated at ambient conditions, 86.3 GPa, and 130.8 GPa. The error bars indicate 3σ of peak fitting error.



## Supplementary Information References

- Ghosh, D.B., Karki, B.B. (2018) First-principles molecular dynamics simulations of anorthite ( $\text{CaAl}_2\text{Si}_2\text{O}_8$ ) glass at high pressure. *Physics and Chemistry of Minerals* 45, 575–587.
- Kono, Y., Park, C., Kenney-Benson, C., Shen, G., Wang, Y. (2014) Toward comprehensive studies of liquids at high pressures and high temperatures: Combined structure, elastic wave velocity, and viscosity measurements in the Paris-Edinburgh cell. *Physics of the Earth and Planetary Interiors* 228, 269–280.
- Kono, Y., Kenney-Benson, C., Ikuta, D., Shibasaki, Y., Wang, Y., Shen, G. (2016) Ultrahigh-pressure polyamorphism in  $\text{GeO}_2$  glass with coordination number >6. *Proceedings of the National Academy of Sciences of the United States of America* 113, 3436–3441.
- Kono, Y., Shibasaki, Y., Kenney-Benson, C., Wang, Y., Shen, G. (2018) Pressure-induced structural change in  $\text{MgSiO}_3$  glass at pressures near the Earth's core–mantle boundary. *Proceedings of the National Academy of Sciences of the United States of America* 115, 1742–1747.
- Petitgirard, S., Malfait, W.J., Sinmyo, R., Kuppenko, I., Hennem, L., Harries, D., Dane, T., Burghammer, M., Rubie, D.C. (2015) Fate of  $\text{MgSiO}_3$  melts at core–mantle boundary conditions. *Proceedings of the National Academy of Sciences of the United States of America* 112, 14186–14190.
- Petitgirard, S., Malfait, W.J., Journaux, B., Collings, I.E., Jennings, E.S., Blanchard, I., Kantor, I., Kurnosov, A., Cotte, M., Dane, T., Burghammer, M., Rubie, D.C. (2017)  $\text{SiO}_2$  glass density to lower-mantle pressures. *Physical Review Letters* 119, 215701.
- Rosales-Sosa, G.A., Masuno, A., Higo, Y., Inoue, H. (2016) Crack-resistant  $\text{Al}_2\text{O}_3$ – $\text{SiO}_2$  glasses. *Scientific Reports* 6, 23620.
- Prescher, C., Prakapenka, V.B., Stefanski, J., Jahn, S., Skinner, L.B., Wang, Y. (2017) Beyond sixfold coordinated Si in  $\text{SiO}_2$  glass at ultrahigh pressures. *Proceedings of the National Academy of Sciences of the United States of America* 114, 10041–10046.
- Sato, T., Funamori, N. (2010) High-pressure structural transformation of  $\text{SiO}_2$  glass up to 100 GPa. *Physical Review B* 82, 184102.
- Shen, G., Prakapenka, V.B., Rivers, M.L., Sutton, S.R. (2003) Structural investigation of amorphous materials at high pressures using the diamond anvil cell. *Review of Scientific Instruments* 74, 3021–3026.
- Tsuchiya, T. (2003) First-principles prediction of the  $P$ - $V$ - $T$  equation of state of gold and the 660-km discontinuity in Earth's mantle. *Journal of Geophysical Research* 108, 2462.

